How Small-World Interactions Can Lead to Improved Quantum Annealer Designs

Helmut G. Katzgraber and M.A. Novotny

Phys. Rev. Applied **10**, 054004 — Published 2 November 2018

DOI: 10.1103/PhysRevApplied.10.054004

How small-world interactions can lead to improved quantum annealer designs

Helmut G. Katzgraber[1, 2, 3, 4] and M. A. Novotny[5, 6, 7, *]

[1] *Microsoft Quantum, Microsoft, Redmond, WA 98052, USA*
[2] *Department of Physics and Astronomy, Texas A&M University, College Station, Texas 77843-4242, USA*
[3] *1QB Information Technologies (1QBit), Vancouver, British Columbia, Canada V6B 4W4*
[4] *Santa Fe Institute, 1399 Hyde Park Road, Santa Fe, New Mexico 87501, USA*
[5] *Department of Physics and Astronomy, Mississippi State University, Mississippi State, MS 39762-5167, USA*
[6] *HPC² Center for Computational Sciences, Mississippi State University, Mississippi State, MS 39762-5167, USA*
[7] *Faculty of Mathematics and Physics, Charles University, Ke Karlovu 5, CZ-121 16 Praha 2, Czech Republic*

There are many factors that influence the design of quantum annealing processing units. Here we address the issue of improving quantum annealing processing unit designs from the point of view of the critical behavior of spin glasses. It has been argued [Phys. Rev. X **4**, 021008 (2014)] that among the most difficult Ising spin-glass ground-state problems are those related to lattices which exhibit a finite-temperature spin-glass transition. Here, we show that adding small-world couplers between qubits (spins) to the native quasi-planar quantum processing unit graph results in a topology where a disordered Ising system can undergo a finite-temperature spin-glass transition, even when an Ising spin glass on the quasi-planar native graph does not display a transition into a glassy phase at any finite temperature. To ensure that these systems can be engineered with current fabrication techniques, using large-scale Monte Carlo simulations we demonstrate that highly-constrained systems restricted to a few fabrication layers and with fixed coupler angles can also exhibit a finite-temperature spin-glass transition. This indicates that these systems might be mean-field-like, which also means that embedding highly-nonplanar problems might be simplified when compared to the underlying native topology. Our results are illustrated using the quasi-planar Chimera topology currently used in the D-Wave Systems Inc. quantum annealing machines, as well as standard two-dimensional square lattices. The presented approach can be generalized to other topologies.

PACS numbers: 75.50.Lk, 75.40.Mg, 05.50.+q, 03.67.Lx
Keywords: Quantum Computing, Adiabatic Quantum Computing, Ising Spin Glass

I. INTRODUCTION

We are currently in the midst of an exciting and formative era in the emerging field of quantum computing. The first quantum computers are being built and rapidly refined. Quantum computing is rapidly transitioning from a theoretical curiosity to being a practical, indispensable tool on the computational science, engineering, and business workbench. A quantum computer operates on qubits (quantum bits) via quantum operations, as opposed to a classical computer which operates on bits (the binary values 0 and 1). A register of N qubits may simultaneously be in a quantum superposition state of all 2^N possible states [1]. In contrast, a classical computer must always be in one of the possible 2^N states. The ability to operate on qubits rather than bits is what gives the enticing game-changing potential possibilities to quantum computers. Quantum computers hold the promise to be able to have an exponential increase in the ability to calculate solutions to certain problems, as compared to classical computers [1–3].

In any emerging technology, the architectures and underlying materials, as well as the actual engineering process are developed and improved alongside the first operational machines. For example, in 2016 IBM publicly released a gate-model quantum computing device with 5 qubits on a star-shaped topology, while, in parallel an internal version with 16 qubits and a different topology (released in 2017) was being tested [4]. Similarly, whenever D-Wave Systems Inc. releases a new quantum processing unit for their quantum annealing machines, different hardware iterations and graph topologies are tested using different metrics that, likely, range from problem embedability, qubit crosstalk, engineering constraints, coherence times, to application-driven metrics, to name a few.

While digital quantum processing units can be programmed to study a variety of problems, a quantum annealer's main purpose is to find optima for hard binary optimization problems via quantum annealing [5–11]. The architecture of the quantum annealing machine may be viewed as the arrangement of qubits at the vertices (nodes) of a graph, and the bonds of the undirected graph are the couplers (or interconnects) between the qubits. Programming a quantum annealer consists in providing a bias field h_i for each qubit i, as well as the sign and magnitude of the interactions between pairs of qubits i and j, the coupling strength and sign of the coupler J_{ij}. Any problem in a quadratic binary unconstrained format can then be embedded onto the device's topology. For native problems, i.e., without embedding,

* man40@msstate.edu

the nonplanarity of the quantum annealer graph, together with both possible signs of the coupling between qubits, can lead to frustration in the encoded spin-glass-like problem, which can, potentially make the finding of the ground state an NP-hard problem [12, 13].

Recently, multiple types of synthetic benchmark problems have emerged [14–18] in an effort to demonstrate that D-Wave quantum annealing machines can outperform algorithms on classical CMOS hardware. Although to date only a verifiable constant speedup has been found [19] and applications have only yielded mixed results [20–25], there is still much effort into elucidating an application scope of the D-Wave device. While synthetic benchmarks designed to "break" classical algorithms represent excellent benchmark problems, their most prominent drawback is the need to encode a hard logical problem into the physical hardware layout of the quantum annealing processing unit (QAPU). This overhead often results in considerably smaller logical problems that might be far from the asymptotic regime where the true scaling sets in. As such, it is desirable to develop native benchmark problems that use all qubits on the QAPU, and that are computationally tunable and ideally hard. While this is not easily accomplished with current hardware [26], it might be possible with better hardware designs, as proposed in this work.

Defining and detecting quantum speedup is an intricate task [27]. Quantum speedup is one component in the search for quantum supremacy. Quantum supremacy may be defined as the point where a quantum computer can perform tasks more efficiently than a classical computer. This can be, for example, faster than current computer technologies, using considerably less memory, or simply tasks that cannot be simulated on classical hardware at all. As the problem size and classical computer hardware are scaled up, it is expected that the resource requirements for quantum hardware are considerably less, i.e., the quantum computer outperforms classical hardware by an even larger margin. For quantum annealers, being able to more efficiently embed problems (i.e., with a smaller embedding overhead) that might either show any quantum advantage or speedup in the native architecture of the QAPU plays a central role in the the assessment of the potential of such devices. It is this component on which we concentrate in this article.

Although there are many metrics that, in principle, drive the design of a particular quantum chip topology, because no definite application-based signs of quantum speedup exist to date, we focus on well-understood *native* [28] fundamental spin-glass benchmarks in an effort to "tickle" any advantage out of the available hardware. It has been argued in the past [26] that Ising spin-glass problems might pose greater challenges to optimization machines, as well as classical algorithms, if the underlying optimization problem undergoes a finite-temperature spin-glass transition where the barriers in the free-energy landscape are more prominent at low close-to-zero temperatures. Similar arguments hold for graphs with higher connectivity [29]. Quantum processing units tend to have a planar topology, mainly due to fabrication constraints. Because spin glasses on quasi-two-dimensional topologies—such as the $K_{4,4}$-based Chimera graph [30] of the D-Wave devices—do not have a finite-temperature spin-glass transition, here we outline an approach to induce finite-temperature transitions, as well as mean-field-like behavior for spin glasses on quasi-planar topologies by adding (constrained) small-world couplers [31, 32]. While a finite-temperature spin-glass transition allows for the development of more elaborate benchmarking techniques, the small-world properties of the QAPU topology that lead to mean-field critical behavior potentially assists with the embedding of nonplanar problems in the hard-wired topologies of these systems. We illustrate the proposed approach using D-Wave's Chimera graph (see Fig. 1) and demonstrate that the approach is generic by also studying a two-dimensional square lattice.

We argue that the graph of any QAPU should allow one to study optimization problems that map onto a spin-glass model above the upper critical dimension $d_{\rm upper}$. For an Ising spin glass $d_{\rm upper} = 6$ [34]. For a graph with $d \geq d_{\rm upper}$ the critical exponents are those of a mean-field model, namely the same as having every qubit interacting with every other qubit [34]. A graph which has a three-dimensional cubic structure, for example, will never be able to embed a computational problem which corresponds to a six-dimensional hypercube without a large overhead. Unfortunately, for mostly engineering reasons, building a QAPU with a hypercube in six or more dimensions is not feasible at the moment. The approach presented here whereby small-world (SW) connections [31] are added to the underlying problem graph potentially enables an economic route to build QAPUs for problems that map onto spin glasses on topologies that are above the upper critical dimension. This small-world-enhanced architecture is related to the architectures of perfectly scalable classical massively-parallel computers [35, 36]. Our study thus enables us to establish a reasonable requirement for the architecture of any QAPU [37]. Trying to engineer a QAPU with unconstrained small-world interactions may well be unrealistic (see Fig. 2), because for k randomly-placed additional small-world couplers worst-case k additional fabrication layers are needed. Consequently a large portion of the paper is devoted to investigating whether constrained small-world connections are sufficient to obtain both a finite-temperature spin-glass transition and associated mean-field spin glass critical exponents.

For ferromagnetic models, the addition of small-world bonds has been studied both theoretically and by computer simulations [38–43]. The small-world bonds can

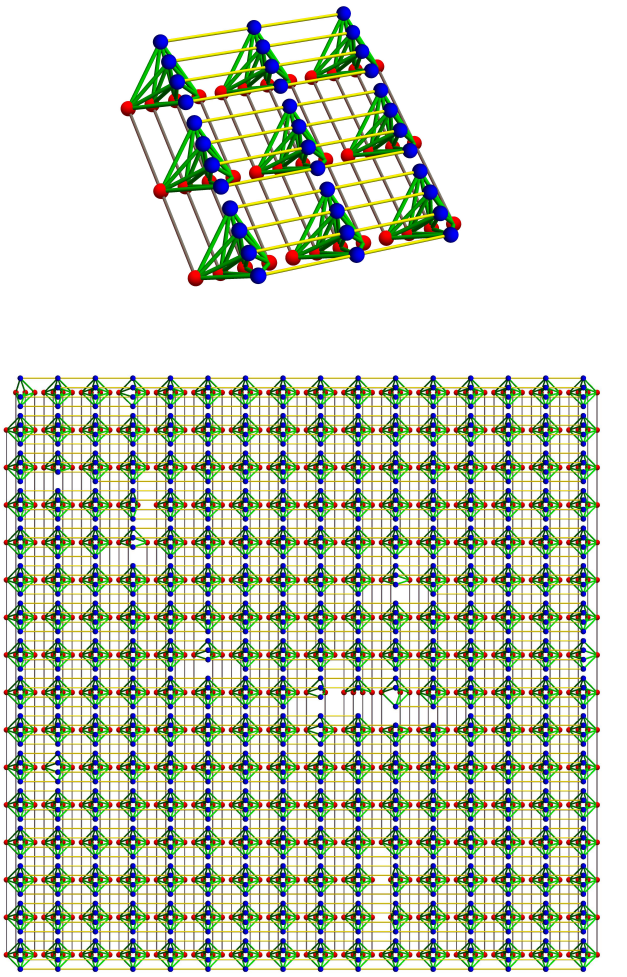

FIG. 1. $K_{4,4}$ Chimera lattices with $N = 8L^2$ sites, illustrated as a quasi-two-dimensional (referred to as "two-level") system. Every unit cell has four qubits in the upper layer (blue spheres) and four qubits in the lower layer (red spheres), and the intra-unit-cell couplers have each of the top four qubits connected to every one of the four lower sites (green cylinders). The inter-unit-cell connections in the top layer (yellow cylinders) and the bottom layer (gray cylinders) are shown. The graph has free boundary conditions. The top panel depicts a Chimera graph with $L = 3$ and the bottom panel depicts the Chimera graph of a current 2000Q model (top view) with $L = 16$ and some missing qubits and couplers (of the $N = 2048$ available qubits only 2023 are operational). The supplemental material contains three-dimensional interactive versions of these graphs [33].

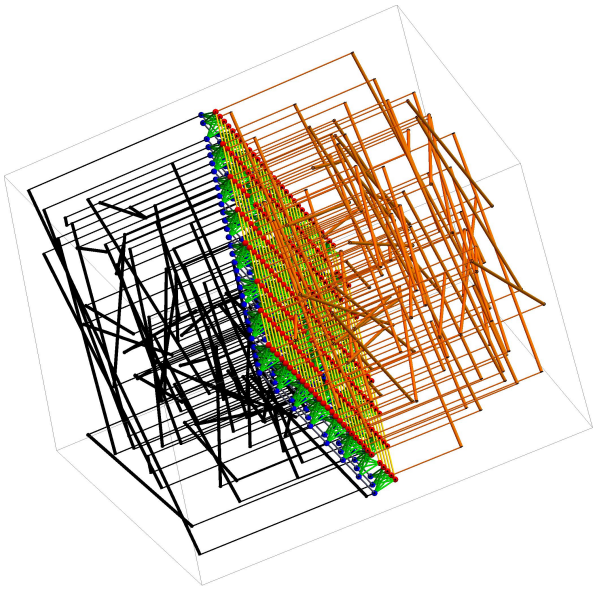

FIG. 2. A $K_{4,4}$ Chimera lattice with $L = 8$ ($N = 512$ sites) and with added small-world couplers, illustrated as a two-level system. Rendered is an actual D-Wave Two chip with 489 working qubits and 1345 operational couplers. Every unit cell has four qubits in the upper layer (blue spheres) and four qubits in the lower layer (red spheres), together with each of the top four qubits connected to every one of the four lower qubits (green cylinders). The inter-unit-cell connections in the top layer (yellow cylinders) and the bottom layer (gray cylinders) are shown. The graph has free boundary conditions. Qubits on the top (bottom) layer have an additional 64 small-world couplers depicted as orange (black) cylinders. The only constraint on the small-world couplers is that each qubit can have at most one additional small-world coupler. To keep the connections from overlapping, every small-world coupler is at a different height above or below the qubit planes. The supplemental material contains a three-dimensional interactive file for this graph [33].

be added by starting, for example, with either a one-dimensional or two-dimensional regular lattice. The consensus which has emerged is the addition of the small-world bonds gives a finite-temperature transition, even starting from a regular one-dimensional lattice which does not have a finite critical temperature, and furthermore the exponents associated with the critical behavior [32, 44, 45] have mean-field behavior, namely the same as associated with ferromagnetic models above the upper critical dimension $d_{\rm upper}^{\rm (ferro)} = 4$. For the ferromagnet, finite-size scaling of both the ferromagnetic Binder cumulant and ferromagnetic susceptibility gives the mean-field exponents $\nu_{d\geq 4}^{\rm (ferro)} = 2$ and $\gamma_{d\geq 4}^{\rm (ferro)} = 1$. More information on additional features of small-world networks can be found in Refs. [31, 46–50].

The paper is structured as follows. Section II introduces the Ising spin glass Hamiltonian, the graphs used in our studies (Chimera and square lattices with and without small-world connections), and computational methodologies used to study a potential spin-glass transition using finite-size scaling. Section III contains results for unconstrained small-world connections added to Chimera graphs. Results of adding small-world connections to Chimera graphs with constraints are presented in Sec. IV for constraints to a small number of layers and in Sec. V for constraints also confined to a $\pm\pi/4$ angle. Section VI contains results for a square lattice with added connections constrained to both a small number of layers

and to angles of $\pm\pi/4$. Discussions and conclusions are contained in Sec. VII.

II. MODEL AND METHODS

We consider a graph G with N nodes, where the QAPU qubits reside on the vertices of the graph. Graph edges represent the couplers between the qubits. In this work we study a spin glass on the native topology of the QAPU, i.e.,

$$\mathcal{H} = -\sum_{i,j=1}^{N} J_{ij} S_i S_j. \tag{1}$$

Here, $S_j \in \{\pm 1\}$ represent Ising spins. The couplers J_{ij} of the native graph are chosen from a Gaussian distribution with zero mean and standard deviation 1. The additional small-world couplers (explained in detail below) are chosen from a bimodal distribution, i.e., $J_{ij} \in \{\pm 1\}$ with equal probability to somewhat accommodate the fact that the engineering and calibration of the additional small-world couplers is more complex than the native couplers of the native QAPU graph. We work only with 2-local graphs in this paper, leaving a discussion of k-local ($k > 2$) graphs to Sec. VII. The (nonplanar) graphs studied have cycles (closed paths along the bonds) and the couplings can have both signs, in general, therefore not all bonds can simultaneously be satisfied by an arrangement of the N values of S_j, thus leading to frustration. This also means that finding the ground-state of these systems is an NP-hard problem [12, 13]. Because an existence of a stable spin-glass state in a field for short-range systems remains controversial [51–54], without loss of generality we focus here on spin glasses without local biases (fields).

We do note, however, that nonzero biases (which, incidentally, could lead to interesting benchmark designs in the search for quantum speedup) play an important role in applications. In Ising systems, the introduction of biases can change the complexity class of the problem. Mean-field Ising spin glasses, however, exhibit a finite-temperature spin-glass transition for biases and temperatures below the de Almeida-Thouless line [55]. This means that for small enough biases, a spin-glass phase will be present when the system is in the mean-field regime, i.e., when small-world couplers are added. While infinitesimal biases would destroy the fragile spin-glass state on short-range topologies such as the Chimera topology, the addition of small-world couplers would make the resulting spin-glass state on such lattices more stable against local qubit noise, i.e., random biases. Similarly, if the critical scaling is mean-field like for zero bias fields, one expects the same for the case with bias fields, as both have the same spin glass upper critical dimension $d_{\text{upper}} = 6$.

For a spin glass, the canonical order parameter is the spin overlap defined as

$$q = \frac{1}{N}\sum_{j=1}^{N} S_j^{(\alpha)} S_j^{(\beta)}. \tag{2}$$

Here, "(α)" and "(β)" represent two copies of the system with the same disorder. It is convenient to construct dimensionless quantities from the order parameter in Eq. (2) to better pinpoint the location of a phase transition. The Binder ratio is such a dimensionless function, which means that, at a putative transition, data for different system sizes N will cross when $T = T_c$, where T_c is the critical temperature (up to corrections to scaling). Defined via

$$g = \frac{1}{2}\left(3 - \frac{[\langle q^4\rangle]_{\text{av}}}{[\langle q^2\rangle]^2_{\text{av}}}\right), \tag{3}$$

the Binder ratio scales as

$$g \sim G\left[N^{1/\nu_{\text{eff}}}\,(T - T_c)\right] \equiv G\,(x)\,, \tag{4}$$

where $x = N^{1/\nu_{\text{eff}}}\,(T - T_c)$. In Eq. (3) the angular brackets $\langle\cdots\rangle$ represent a thermal average and the square brackets $[\cdots]_{\text{av}}$ a configurational average. Note that the configurational average is over coupler values when only the native graph is studied. However, in the case where small-world couplers without restrictions are added to the native graph, the average is over coupler values, as well as the position of the small-world couplers. We note that for the restricted simulations a *fixed* set of small-world couplers is used, i.e., again the configurational average is only over the values of the couplers. The effective critical exponent ν_{eff} is given via

$$\nu_{\text{eff}} = \begin{cases} \nu & d_{\text{l}} < d \le d_{\text{u}} \\ \nu_{\text{MF}} & d \ge d_{\text{u}}. \end{cases} \tag{5}$$

Note that in Eq. (5) $\nu_{\text{MF}} = 3$. For spin glasses, the upper critical dimension is $d_{\text{u}} = 6$ [34, 56] and the lower critical dimension d_{l} lies between 2 and 3 [57, 58] with a commonly-used value being 5/2 [57]. From Eq. (4) the critical parameters ν_{eff} and T_c can be estimated via a finite-size scaling analysis [59]. For a hypercubic lattice with short-range interactions $L = N^{1/d}$, with d the space dimension. Often finite-size scaling equations are written in terms of L. Here, however, because of the added small-world couplers a space dimension d is somewhat ill defined and thus we write all expressions in terms of N.

In a mean-field like system the critical exponent η associated with the susceptibility is known a priori and can be expressed in terms of ν_{MF}. Therefore, to obtain an independent estimate of a transition we also study the finite-size scaling of the spin-glass susceptibility

$$\chi/N = [\langle q^2\rangle]_{\text{av}} \;\sim\; N^{-\Gamma}\,X\,(x)\,, \tag{6}$$

where Γ is an independent critical exponent. Reference [60] adds support to the prediction that above d_{u} one

expects

$$\Gamma = \frac{\gamma_{\mathrm{BP}} + 2\beta_{\mathrm{BP}}}{d_{\mathrm{u}}\nu_{\mathrm{MF}}} = \frac{2}{3}, \tag{7}$$

where the subscript "BP" stands for bootstrap percolation [61]. Therefore, plotting $\chi/N^{1/3}$ as a function of x should generate the scaling function X if the correct critical temperature T_{c} is used.

Simulations are performed using parallel tempering Monte Carlo [62]. Note that for each disorder instance we simulate two independent replicas to compute the spin-glass overlap. We test thermalization using the method developed in Ref. [63] adapted to the Chimera topology. In all simulations, open boundary conditions are used to mirror current planar chip designs.

III. CHIMERA LATTICE WITH UNCONSTRAINED SMALL-WORLD COUPLERS

The Chimera lattice [30] (see Fig. 1) does not have a finite-temperature spin-glass transition [26]. As a first step, to verify that a finite-temperature phase transition in the mean-field universality class can be induced in a quasi-planar topology, we add unrestricted small-world couplers to the lattice, depicted in Fig. 2. We study lattices with $L \times L$ unit cells of 8 sites each, i.e., $N = 8\,L^2$ sites.

In the simulations, for each number of sites $N \in \{1152, 1568, 2048, 2592\}$ we thermalize the system for 2^{20} Monte Carlo sweeps and measure over the same amount of sweeps. For the parallel tempering scheme we use 30 temperatures in the range $T \in [0.9620, 2.3825]$. Configurational averages are performed over approximately 5000 samples.

A. Algorithm to add small-world couplers

The added small-world couplers can take the values $J_{ij} \in \{\pm 1\}$ with equal probability. We only apply one restriction to the small-world couplers, namely that each site on the native Chimera graph can have at most *one* additional small-world coupler. The small-world couplers that connect two qubits which either both lie in the top layer or both lie in the bottom layer of the Chimera lattice are shown in Fig. 1. The algorithm to place $n_{\mathrm{SW}}/2$ couplers on the top or bottom layer of Chimera is as follows. Randomly choose two sites in a given layer which do not yet have a small-world connection and add a small-world coupler between them until there are n_{SW} couplers either in the top or bottom layer. Note that $n_{\mathrm{SW}} \leq N/4$, because the Chimera graph has a two-layer structure and every coupler connects two sites. In Fig. 2 each small-world coupler is placed at a different level above the top qubit layer (below the bottom qubit layer) in order to prevent small-world couplers from intersecting (a no-crossing constraint). As N increases the number of small-world couplers is increased proportionally, so every lattice has the same fraction of small-world couplers to qubits. This also means that the number of additional fabrication layers for a chip design grows accordingly.

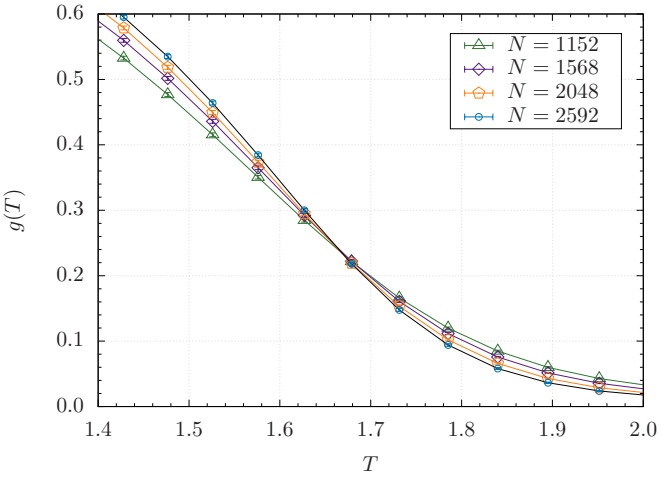

FIG. 3. Binder cumulant g [Eq. (3)] as a function of temperature T for a spin glass on a Chimera lattice with added unconstrained small-world interconnects (see Fig. 2). Data for different system sizes N cross, suggesting the existence of a finite-temperature spin-glass transition.

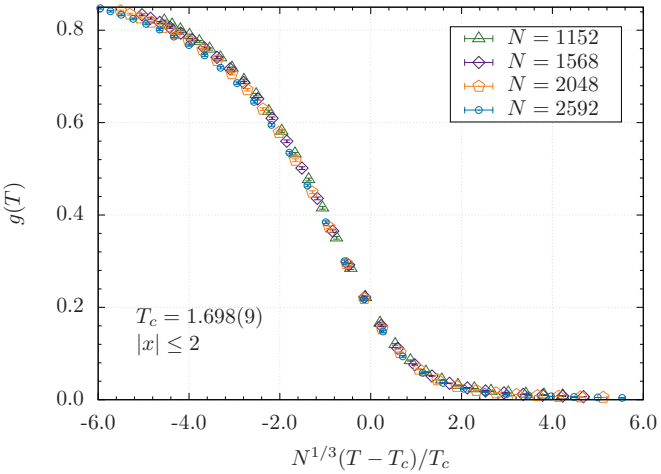

FIG. 4. Finite-size scaling of the data presented in Fig. 3 according to Eq. (4). The critical exponents are fixed to the mean-field values and only the critical temperature T_{c} is a free parameter. The data scale well for $|x| \leq 2$ and we estimate $T_{\mathrm{c}} = 1.698(9)$.

B. Results

Figure 3 shows results for the Binder cumulant g for the spin-glass order parameter. The crossing for different N suggest a finite-temperature spin-glass transition. This means that the addition of small-world couplers to a Chimera lattices generates a topology where a spin glass can have a finite-temperature transition. Figure 4 shows a finite-size scaling of the data in Fig. 3. The scaling of the data is restricted to a window $|x| \leq 2$ and $\nu_{\rm eff} = \nu_{\rm MF} = 3$ fixed. The data scale well and we estimate $T_{\rm c} = 1.698(9)$. To corroborate these results, Fig. 5 shows a finite-size scaling of the spin-glass susceptibility according to Eq. (6) with again the critical exponents fixed to the mean-field values. The data scale well and we find $T_{\rm c} = 1.705(10)$, which agrees within error bars with the estimate obtained from the Binder ratio. We have also performed the scaling analysis with the different scaling exponents as free parameters and obtain estimates for the critical temperature that agree within error bars with the aforementioned estimates, as well as estimates for the critical exponents that agree with the mean-field values within error bars. Therefore adding small-world couplers to a Chimera lattice would allow studies of J_{ij} arrangements which have characteristics of those of short-range spin glasses with dimensions $d \geq 6$. This also means that a spin-glass state in a field might be possible in such architectures.

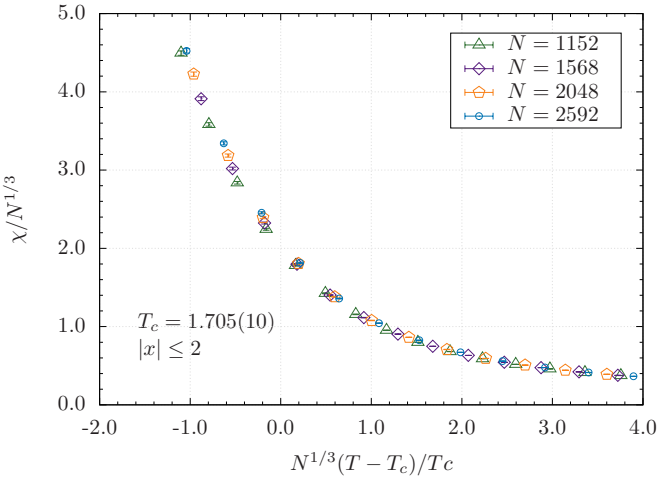

FIG. 5. Finite-size scaling of the spin-glass susceptibility χ according to Eq. (6). The critical exponents are fixed to the mean-field values and only the critical temperature $T_{\rm c}$ is a free parameter. The data scale well for $|x| \leq 2$ and we estimate $T_{\rm c} = 1.705(10)$, in agreement within error bars with the estimate from the Binder ratio (see Fig. 4).

We note that the data in Figs. 3 through 5 were for complete Chimera lattices with no vacancies. We also performed simulations where the Chimera lattices has a small fraction of vacancies – as commonly found in QAPUs – and averaged over these vacancy arrangements. Again, the scaled data exhibit a clear finite-temperature spin-glass transition with exponents expected for a spin glass in the mean-field regime (not shown).

Figures 3 through 5 are for small-world connections added to Chimera graphs. These figures should be contrasted with Figure 2 in Ref. [26] for Chimera lattices without any small-world connections. Figure 2 in Ref. [26] shows using a finite-size scaling of both the Binder cumulant and the susceptibility that the transition only occurs at zero temperature.

IV. CHIMERA LATTICE WITH CONSTRAINED SMALL-WORLD COUPLERS

It would be extremely difficult to engineer a QAPU with the unconstrained small-world interconnects depicted in Fig. 2, because the number of fabrication layers (the number of layers the small-world couplers with a no-crossing constraint in every fabrication layer) required would grow rapidly with the number of qubits N. Therefore, we also investigate the results of placing further constraints on the couplers added to the underlying Chimera lattice. In this section we constrain the number of fabrication layers, with the non-intersecting condition, the added couplers can have.

Fig. 6 shows a $K_{4,4}$ Chimera lattice with $L = 20$, and added small-world couplers, with four added layers (two above the layer of the top qubits and two below the layer of the bottom qubits). The Chimera lattice is depicted as a two-level system. Every Chimera lattice unit cell has four qubits in the upper layer and four qubits in the lower layer, together with each of the top four qubits connected to every one of the four lower qubits. The intra-unit-cell connections in the top layer and the bottom layer are shown. The graph has free boundary conditions. For details and a better view of the different couplers and qubit, see Fig. 1. Here we use the same color coding for the different qubits and couplers for the native graph. In addition, small-world couplers are added in four additional layers, two above and two below the qubit planes. In this example, the top qubits are connected by 398 small-world couplers (red and black cylinders), and the bottom qubits by 398 small-world couplers (maroon and cyan cylinders). To keep the connections from overlapping, every small-world layer is at a different height above or below the qubit layers.

A. Algorithm to add small-world couplers

The constraint of the added couplers is that at most one small-world coupler can be connected to any qubit, that there can be only four additional layers (two above the top qubit layer and two below the bottom qubit layer), and the added connections must not intersect

within a layer. The small-world couplers are added iteratively. For $n_{\rm SW}/2$ connections for the top or bottom layer qubits the iterative procedure is as follows.

1. Select at random two qubits in the layer which do not yet have a small-world coupler.

2. Attempt to join the two chosen qubits with a small-world coupler. If the attempted small-world coupler has a slope which is non-negative and does not intersect any small-world couplers that already have been added to the first layer for small-world couplers, add this small-world coupler to the first small-world layer and to the graph. If the attempted small-world coupler has a slope which is non-positive and does not intersect any other small-world couplers which already have been added to the second layer for small-world couplers, add this small-world coupler to the second small-world layer and to the graph. If the attempted connection cannot be placed in either layer of small-world couplers without intersecting existing couplers, discard this attempt and return to step 1.

The total number of added couplers before no additional ones can be added depends on the order of the randomly-chosen qubits, with the upper bound $n_{\rm SW} \leq N/2$. The slopes of the added couplers are calculated with the x axis in Fig. 6 being horizontally left-to-right, and the y axis being vertically down-to-up. An attempted coupler with an infinite slope or zero slope is allowed to be added to either layer, and an attempt to add it to each layer is performed.

The fabricated chip of a D-Wave machine with a Chimera graph has a bottom layer of qubits placed on a substrate surface, with a top layer of qubits placed in a fabrication layer above the first. Consequently, it may be difficult to fabricate a graph based on a Chimera lattice with added layers both above and below the fabrication layers for the Chimera lattice. Therefore, we also performed calculations to study architectures with added couplers only attached to the top layer of qubits. An example of a two layer system is shown in Fig. 7 for $L = 16$. The Chimera graph has the same structure as in Fig. 6. Small-world couplers are added, constrained to be in only two layers (both above the Chimera plane of the top qubits). The top qubits are connected by 127 small-world couplers (red cylinders) in the first layer, and 127 qubits (black cylinders) in the second layer. To keep the connections from overlapping, each small-world layer is at a different height above the top qubit plane.

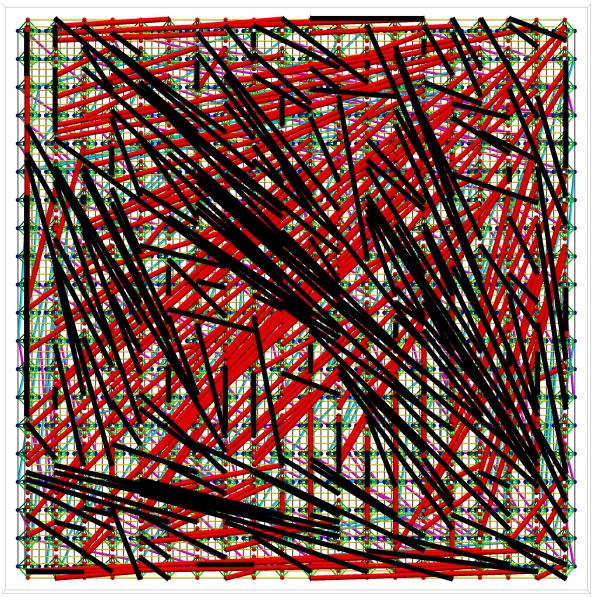

FIG. 6. Chimera lattice ($L = 20$) and added small-world connections constrained to four layers (two above and two below the standard Chimera topology). The supplemental material contains three-dimensional interactive versions of these graphs [33].

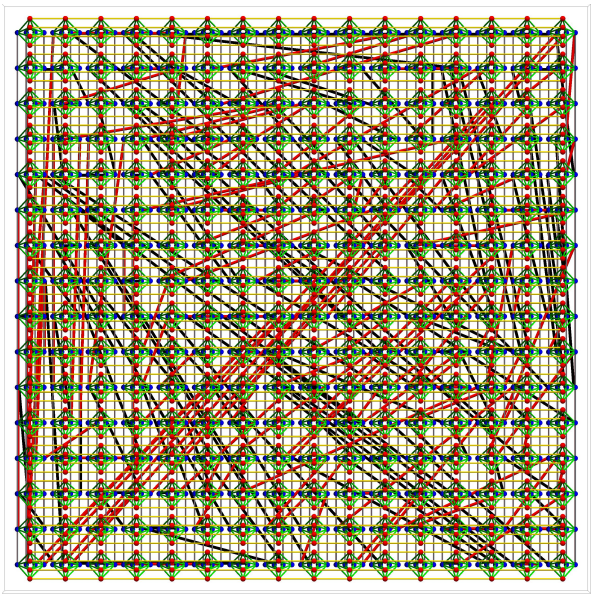

FIG. 7. Chimera lattice ($L = 16$) and added small-world connections constrained to two layers above the standard qubit planes. The supplemental material contains three-dimensional interactive versions of these graphs [33].

B. Results

For both the case of four (Fig. 6) and two (Fig. 7) additional layers we performed large-scale Monte Carlo calculations as outlines in Sec. III. Averaging over both coupler values and different coupler distributions resulted

again in a finite-temperature spin-glass transition. However, the latter is unrealistic, because the chip design should be static. Fixing the coupler positions and performing simulations where the configurational average is only over coupler values resulted in some cases where a possible transition was observed and others where this was not the case (not shown). Clearly, the strong fluctuations in the position of the couplers thus resulted in lattices that might have been at times mean-field like and at other times not. This effect is far more pronounced in the system with two additional layers, which is why we next focus on the system with four additional layers. Furthermore, additional constraints on the small-world couplers are clearly needed to ensure that a reproducible spin-glass transition is found and to reduce these strong corrections to scaling.

V. CHIMERA LATTICE WITH ANGLE CONSTRAINED SMALL-WORLD COUPLERS

Fabricating systems as depicted in Figs. 6 or 7 may still be difficult. Furthermore, tuning the qubits to be within desired specifications for a QAPU may be extremely difficult for such graphs. In an effort to also reduce the fluctuations and seemingly random results obtained in Sec. IV, we study the effects of the further constraint of having all added couplers having slopes of either $+1$ or -1 (angles formed of $+\pi/4$ or $-\pi/4$). The slopes are calculated only from the unit cells, not from specific positions of the qubit locations within a unit cell. An example graph with four added layers is shown in Fig. 8. The procedure to add the small-world couplers is the same as outlined in in Sec. IV A, but with the added rejection step the first layer added connections must form an angle of $+\pi/4$ and the second layer added connections must have an angle of $-\pi/4$.

We perform large-scale Monte Carlo simulations for system sizes $N = 8 \cdot L^2$ with $L \in \{16, 18, \ldots, 28, 30\}$ (i.e., $N = 2048, \ldots, 7200$) and thermalize for 2^{23} Monte Carlo sweeps and measure for the same amount of sweeps. For the parallel tempering scheme we use 30 temperatures in the range $T \in [1.5, 2.3]$. Configurational averages are performed over approximately 5000 samples for each system size. The additional number of small-world couplers for each system size is $n_{\rm SW} = 4(L^2 - 1)$.

Figure 9 shows results for the Binder cumulant g for the spin-glass order parameter. The crossing for different N suggest a finite-temperature spin-glass transition for $T \approx 1.88$. Compared to the unrestricted case, corrections to scaling are evident, however much smaller than in Sec. IV. We note that this is likely also enhanced due to the open boundaries. We decided not to use periodic boundaries as we wanted to demonstrate that the proposed approach works for realistic hardware graphs. This means that even for highly-restricted small-world couplers a finite-temperature spin-glass transition can be induced for a spin-glass on the Chimera lattice. To overcome the strong corrections to scaling, we fit the data in Fig. 9 with the known mean-field critical exponents, namely $\nu_{\rm eff} = 3$ and $\Gamma = 2/3$ and only focus on the largest system sizes simulated. Figure 10 shows a finite-size scaling of the data for the Binder ratio. The data have been scaled for $|x| \leq 4$ and scale well. We have also performed a scaling of the data with the critical exponent ν as a variable. The results obtained agree with the exact mean-field value within error bars, however, these are relatively large. Figure 11 shows scaled data for the susceptibility χ using the expected mean-field exponents. The scaling is good and from the scaling of both the Binder ratio and the susceptibility we estimate $T_{\rm c} = 1.88(1)$. Again, allowing the exponents to fluctuate results in estimates with large error bars.

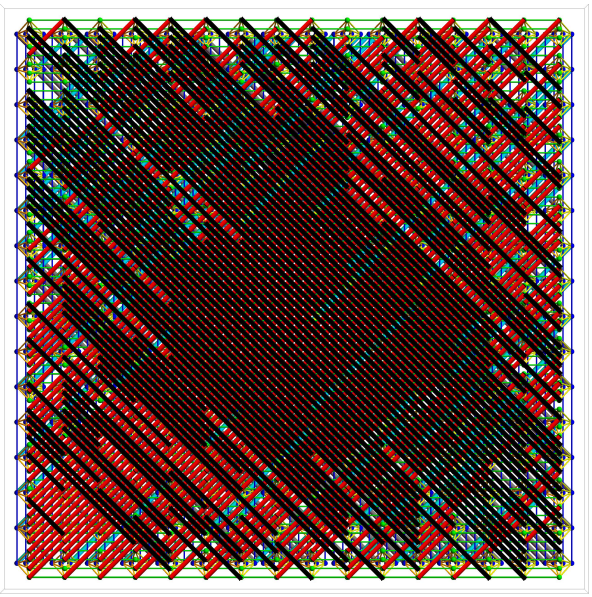

FIG. 8. Chimera lattice ($L = 16$) with added small-world couplers on four layers (two on top and two below), with the connections constrained to diagonal directions. The lattice has $N = 2048$ qubits, 12032 couplers, and additional $n_{\rm SW} = 1020$ small-world couplers (255 per layer). The supplemental material contains three-dimensional interactive versions of these graphs [33].

VI. SQUARE LATTICES WITH ANGLE CONSTRAINED SMALL-WORLD COUPLERS

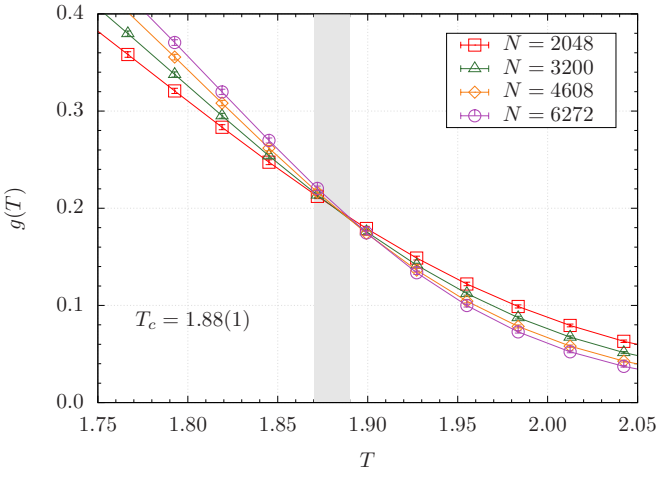

FIG. 9. Binder cumulant g [Eq. (3)] as a function of temperature T for a spin glass on a Chimera lattice with added angle constrained small-world interconnects (see Fig. 8). Data for different system sizes N cross, suggesting the existence of a finite-temperature spin-glass transition. Note that corrections to scaling are large.

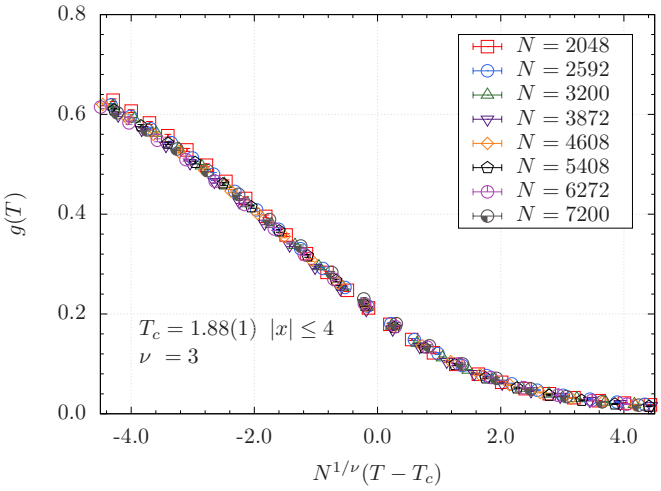

FIG. 10. Finite-size scaling of the data presented in Fig. 9 according to Eq. (4). The critical exponents are fixed to the mean-field values and only the critical temperature T_c is a free parameter. The data scale well for $|x| \leq 4$ and we estimate $T_c = 1.88(1)$.

We demonstrate the generality of the approach and study the effects of open boundary conditions and constrained additional couplers on the scaling and perform large-scale Monte Carlo simulations on square lattices. As for the Chimera lattice we use free boundary conditions. The lattices have $N = L^2$ qubits with L the linear size. Each qubit which is not on the lattice boundary has 4 couplers to its nearest-neighbor qubits. The added small-world couplers are constrained to four layers (two on each side of the lattice) and to having slopes of ± 1, i.e., along the diagonals as in Sec. V for Chimera lattices. The bipartite (red-black checkerboard) nature of the square

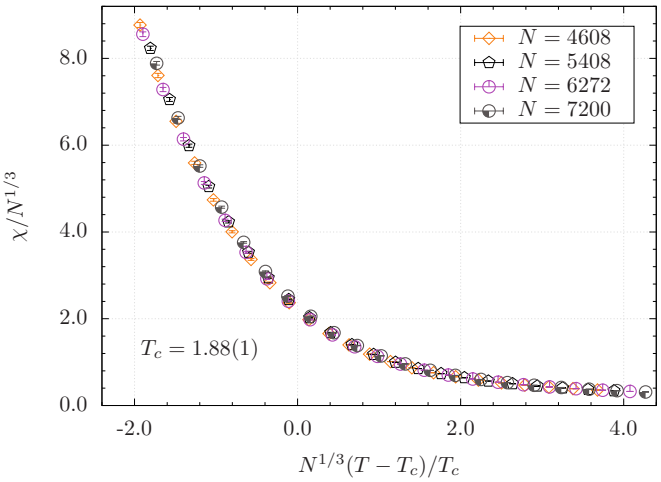

FIG. 11. Finite-size scaling of the spin-glass susceptibility χ according to Eq. (6). The critical exponents are fixed to the mean-field values and only the critical temperature T_c is a free parameter. The data scale well for $|x| \leq 4$ and we estimate $T_c = 1.88(1)$, in agreement within error bars with the estimate from the Binder ratio (see Fig. 9).

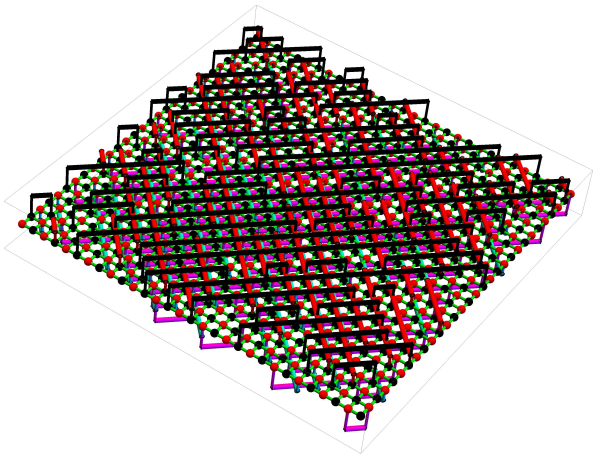

FIG. 12. Square lattice of linear size $L = 30$ with free boundary conditions with added angle constrained small-world couplers. The lattice is bipartite, with the two sublattices having qubits denoted by red or black spheres. The square lattice couplings between qubits are denoted by green bonds. The small-world couplers are constrained to only be along the diagonal and are composed of four layers, each at a different height and of a different color (red, black, cyan, magenta), and each with 50 small-world couplers each. The supplemental material contains a three-dimensional interactive file for this graph [33].

lattice is used to allow for the added connections only between red-red qubits or black-black qubits. This mimics the top-bottom structure used in attaching additional couplers to the qubits of the Chimera lattices. An example square lattice with added small-world couplers is shown in Fig. 12. For all system sizes N simulated, the data are thermalized for 2^{18} Monte Carlo sweeps and

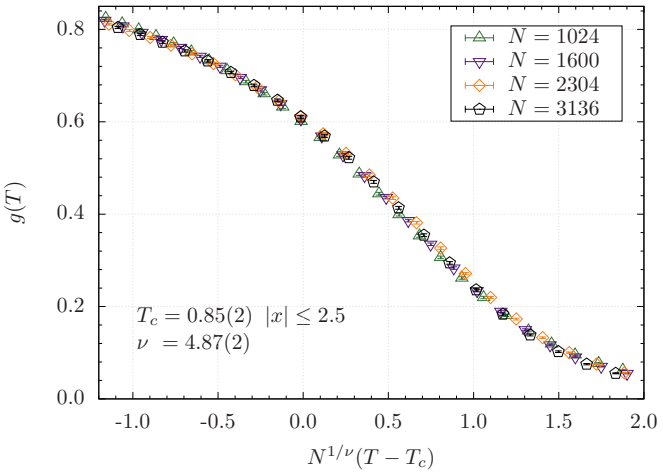

FIG. 13. Finite-size scaling of the Binder cumulant g according to Eq. (4) for a square lattice with angle constrained small-world couplers. The critical exponents are allowed to fluctuate. A scaling for $|x| \leq 2.5$ results in $T_c = 0.85(2)$ with $\nu = 4.87(2)$.

averaged over an additional 2^{18} sweeps. In the parallel tempering method we use 30 temperatures in the range $T \in [0.5, 1.3]$. Configurational averages are performed over approximately 5000 random coupler settings with the location of the small-world couplers fixed for each system size. For a lattice of size $N = L^2$, additional $n_{\rm SW} = N/4$ small-world couplers are added with $n_{\rm SW}/4$ per additional small-world layer.

Figure 13 shows a finite-size scaling of the spin-glass Binder ratio g when both T_c and $\nu_{\rm eff}$ are allowed to be free parameters. The open boundary conditions, together with the constrained added bonds, lead to large corrections to scaling. In fact, the data only scale for $\nu_{\rm eff} = 4.87(2)$ – a value far from the known mean-field value. A scaling of the data for the susceptibility χ was not possible. Corrections to scaling for the square lattice are much higher than for the Chimera lattice when open boundary conditions are used, likely because the number of variables is 8 times smaller. Nevertheless, the data show there is a finite spin-glass transition temperature.

VII. DISCUSSION AND CONCLUSIONS

We have investigated how small-world interactions can lead to improved quantum annealer designs. In particular, we have performed large-scale Monte Carlo simulations of spin-glass models with added small-world couplers. The data are analyzed using a finite-size scaling for both the Binder cumulant g and the spin-glass susceptibility χ. The scaling allows us to determine whether or not there is a finite-temperature spin-glass transition, together with the associated critical exponents that can be used to determine the "meanfieldness" of the Ising spin-glass model on the underlying graph.

Spin-glass models on graphs with added small-world connections have been shown to have a finite spin-glass transition temperature, and the associated critical exponents are those of a mean-field spin glass (or a spin glass above the upper critical dimension $d_{\rm upper} = 6$). Thus small-world graphs should enable an easier embedding of harder spin-glass problems. The ability to more easily embed harder problems, in turn, should aid in the quest for adiabatic quantum machines to show quantum speedup. Furthermore, we have investigated how the addition of a few extra layers in a chip fabrication process, necessitating enforcing constraints on the small-world connections, may also lead to spin-glass critical behavior similar to that of unconstrained small-world connections.

We have first investigated a $K_{4,4}$ Chimera lattice with added small-world couplers. It is known that a spin glass on a $K_{4,4}$ Chimera lattice—such as in Fig. 1—does not exhibit a finite-temperature spin-glass transition [26]. In Sec. III we demonstrate that adding small-world couplers to the Chimera lattice, as in Fig. 2, does result in a finite spin-glass transition temperature. Furthermore, the critical exponents obtained via a finite-size scaling analysis are those expected for an Ising spin glass with a dimension $d \geq d_{\rm upper} = 6$. Therefore, adding small-world couplers to a Chimera lattice should enable the study of more complex optimization problems on a quantum annealer.

In order to bring the graphs into the realm where engineering is possible, we examine constraining the small-world couplers. For the underlying Chimera lattice, in Sec. IV the added connections were constrained to either four or to two additional layers, resulting in disorder-dependent results – an undesirable outcome. In Sec. V the small-world couplers are further constrained to be parallel to the diagonals in the lattice. In this case we obtain again a finite transition temperature in the mean-field regime. We also study the effect of such constrained bonds on an underlying square lattice, Fig. 12 in Sec. VI, where we observe a finite-temperature spin-glass transition. However, corrections to scaling are large and we are unable to verify that the exponents are mean-field.

One can estimate the critical temperature of the spin glass with small-world couplers and compare this to the refrigerator temperature of current quantum annealing machines. For the current D-Wave machine [64], the D-Wave 2000Q with approximately 2000 qubits, the refrigerator temperature is $T_{\rm fridge} = 0.015$K, while the value of the average spin-glass coupling $|J_{ij}|$ is just over 10GHz, i.e., 0.5K. The anticipated spin-glass temperature due to the added small-world couplers, is approximately the same order of magnitude as $|J_{ij}|$. Hence the existence of the finite-temperature spin-glass transition due to small-world connections should be important even for today's early QAPUs, and should contrast sharply with having a graph such as the D-Wave Chimera lattice of the 2000Q

device which does not have a finite-temperature spin-glass transition $0 = T_c < T_{\rm fridge}$. Therefore, for future QAPUs one expects the addition of small-world connections will lead to the relationship between these temperatures of $0 < T_{\rm fridge} << T_c$.

In this study we only analyzed 2-local Hamiltonians. Future annealing machines may have higher-body couplers, and hence the architecture would be associated with hypergraphs. Even in this case, if there is an underlying unit cell with a fixed number $n_{\rm cell}$ of qubits, and the hypergraph has a total number of sites $N = n_{\rm cell}L^d$ (based on a d dimensional lattice) we anticipate that adding small-world couplers could result in a finite-temperature spin-glass transition. For example, in the case of a 3-local lattice a planar triangular lattice has a zero-temperature spin-glass transition [54]. The addition of small-world couplers would likely result in a finite-temperature transition into a spin-glass state.

Further analysis could investigate how the recently-introduced idemetric property (wherein most distances between nodes are almost the same) relates to QAPU designs which can be engineered in a reasonable fashion [65].

Another advantage of lattices enhanced with small-world couplers and their mean-field-like universality class is the possible existence of a spin-glass state in a field. This could be desirable for the generation of more complex synthetic native benchmark problems with local biases and might even help elucidate the behavior of spin glasses in a field via quantum annealing.

ACKNOWLEDGMENTS

H. G. K. would like to thank Andrew Ochoa and Zheng Zhu for multiple discussions and acknowledges the ARC Centre for Excellence in All-Sky Astrophysics in 3D (ASTRO 3D) East Coast Writing Retreat 2018 for support in preparing the manuscript. M. A. N. would like to thank Hans De Raedt, Fenping Jin, Yaroslav Koshka, Kristel Michielsen, and Dilina Perera, for useful discussions. H. G. K. acknowledges support from the NSF (Grant No. DMR-1151387) and thanks Aji Panca and Wilbur Scoville for inspiration. M. A. N. thanks the Faculty of Mathematics and Physics at Charles University for their hospitality during a sabbatical stay, and funding as a Fulbright Distinguished Chair from the Czech Fulbright Commission. M. A. N. carried out part of this work at the Aspen Center for Physics, which is supported by National Science Foundation grant PHY-1607611. We thank the Texas Advanced Computing Center (TACC) at The University of Texas at Austin for providing HPC resources (Stampede Cluster) and Texas A&M University for access to their Ada, and Lonestar clusters. H. G. K.'s research is based upon work supported by the Office of the Director of National Intelligence (ODNI), Intelligence Advanced Research Projects Activity (IARPA), via Interagency Umbrella Agreement No. IA1-1198. M. A. N.'s research is based upon work supported by the Air Force Research Laboratory (AFRL) under agreement number FA8750-18-1-0096. The views and conclusions contained herein are those of the authors and should not be interpreted as necessarily representing the official policies or endorsements, either expressed or implied, of the ODNI, IARPA, AFRL, or the U.S. Government. The U.S. Government is authorized to reproduce and distribute reprints for Governmental purposes notwithstanding any copyright annotation thereon.

[1] N. D. Mermin, *Quantum Computer Science: An introduction* (Cambridge University Press, Cambridge, UK, 2007).

[2] A. de Vries, *Quantum Computation: An Introduction for Engineers and Computer Scientists* (Books on Demand, Norderstedt, Netherlands, 2012).

[3] E. Rieffel and W. Polak, *Quantum Computing: A Gentle Introduction* (MIT Press, Cambridge, MA, 2014).

[4] A. D. Córcoles, E. Magesan, S. J. Srinivasan, A. W. Cross, M. Steffen, J. M. Gambetta, and J. M. Chow, *Demonstration of a quantum error detection code using a square lattice of four superconducting qubits*, Nature Commun. **6**, 6979 (2015).

[5] T. Kadowaki and H. Nishimori, *Quantum annealing in the transverse Ising model*, Phys. Rev. E **58**, 5355 (1998).

[6] T. Kadowaki, *Study of optimization problems by quantum annealing*, Ph.D. thesis, Tokyo Institute of Technology (1998), (quant-ph/0205020).

[7] E. Farhi, J. Goldstone, S. Gutmann, and M. Sipser, *Quantum Computation by Adiabatic Evolution* (2000), arXiv:quant-ph/0001106.

[8] E. Farhi, J. Goldstone, S. Gutmann, J. Lapan, A. Lundgren, and D. Preda, *A quantum adiabatic evolution algorithm applied to random instances of an NP-complete problem*, Science **292**, 472 (2001).

[9] S. Morita and H. Nishimori, *Mathematical Foundation of Quantum Annealing*, J. Math. Phys. **49**, 125210 (2008).

[10] A. Das and B. K. Chakrabarti, *Quantum Annealing and Analog Quantum Computation*, Rev. Mod. Phys. **80**, 1061 (2008).

[11] T. Albash and D. A. Lidar, *Adiabatic Quantum Computing*, Rev. Mod. Phys. **90**, 015002 (2018).

[12] F. Barahona, *On the computational complexity of Ising spin glass models*, J. Phys. A **15**, 3241 (1982).

[13] F. Barahona, R. Maynard, R. Rammal, and J. P. Uhry, *Morphology of ground-states of two-dimensional frustration model*, J. Phys. A **15**, 673 (1982).

[14] I. Hen, J. Job, T. Albash, T. F. Rønnow, M. Troyer, and D. A. Lidar, *Probing for quantum speedup in spin-glass problems with planted solutions*, Phys. Rev. A **92**, 042325

(2015).
[15] A. D. King, T. Lanting, and R. Harris, *Performance of a quantum annealer on range-limited constraint satisfaction problems* (2015), arXiv:1502.02098.
[16] V. S. Denchev, S. Boixo, S. V. Isakov, N. Ding, R. Babbush, V. Smelyanskiy, J. Martinis, and H. Neven, *What is the Computational Value of Finite Range Tunneling?*, Phys. Rev. X **6**, 031015 (2016).
[17] S. Mandrà, Z. Zhu, W. Wang, A. Perdomo-Ortiz, and H. G. Katzgraber, *Strengths and Weaknesses of Weak-Strong Cluster Problems: A Detailed Overview of State-of-the-art Classical Heuristics vs Quantum Approaches* (2016), (arXiv:1604.01746).
[18] S. Mandrà and H. G. Katzgraber, *The pitfalls of planar spin-glass benchmarks: Raising the bar for quantum annealers (again)*, Quantum Sci. Technol. **2**, 038501 (2017).
[19] S. Mandrà and H. G. Katzgraber, *A deceptive step towards quantum speedup detection* (2017), (arxiv:1711.01368).
[20] A. Perdomo-Ortiz, N. Dickson, M. Drew-Brook, G. Rose, and A. Aspuru-Guzik, *Finding low-energy conformations of lattice protein models by quantum annealing*, Sci. Rep. **2**, 571 (2012).
[21] A. Perdomo-Ortiz, J. Fluegemann, S. Narasimhan, R. Biswas, and V. N. Smelyanskiy, *A quantum annealing approach for fault detection and diagnosis of graph-based systems*, Eur. Phys. J., Special Topics **224**, 131 (2015).
[22] E. G. Rieffel, D. Venturelli, B. O'Gorman, M. B. Do, E. M. Prystay, and V. N. Smelyanskiy, *A case study in programming a quantum annealer for hard operational planning problems*, Quant. Inf. Proc. **14**, 1 (2015).
[23] D. Venturelli, D. J. J. Marchand, and G. Rojo, *Quantum Annealing Implementation of Job-Shop Scheduling* (2015), (arxiv:1506.08479).
[24] S. Mandrà, G. G. Guerreschi, and A. Aspuru-Guzik, *Faster than classical quantum algorithm for dense formulas of exact satisfiability and occupation problems*, New J. Phys. **18**, 073003 (2016).
[25] A. Perdomo-Ortiz, A. Feldman, A. Ozaeta, S. V. Isakov, Z. Zhu, B. O'Gorman, H. G. Katzgraber, A. Diedrich, H. Neven, J. de Kleer, et al., *On the readiness of quantum optimization machines for industrial applications* (2017), arXiv:1708.09780.
[26] H. G. Katzgraber, F. Hamze, and R. S. Andrist, *Glassy Chimeras Could Be Blind to Quantum Speedup: Designing Better Benchmarks for Quantum Annealing Machines*, Phys. Rev. X **4**, 021008 (2014).
[27] T. F. Rønnow, Z. Wang, J. Job, S. Boixo, S. V. Isakov, D. Wecker, J. M. Martinis, D. A. Lidar, and M. Troyer, *Defining and detecting quantum speedup* (2014), (arXiv:quant-phys/1401.2910).
[28] In this context, *native* refers to the study of a spin-glass problem on the actual hardware graph without the need of embedding.
[29] D. Venturelli, S. Mandrà, S. Knysh, B. O'Gorman, R. Biswas, and V. Smelyanskiy, *Quantum Optimization of Fully Connected Spin Glasses*, Phys. Rev. X **5**, 031040 (2015).
[30] P. Bunyk, E. Hoskinson, M. W. Johnson, E. Tolkacheva, F. Altomare, A. J. Berkley, R. Harris, J. P. Hilton, T. Lanting, and J. Whittaker, *Architectural Considerations in the Design of a Superconducting Quantum Annealing Processor*, IEEE Trans. Appl. Supercond. **24**, 1 (2014).
[31] D. J. Watts and S. H. Strogatz, *Collective dynamics of 'small-world' networks*, Nature **393**, 440 (1998).
[32] M. B. Hastings, *Mean-Field and Anomalous Behavior on a Small-World Network*, Phys. Rev. Lett. **91**, 098701 (2003).
[33] The supplemental material consists of 7 files in computable document format of the lattices shown in Figs. 1 and 2, 6 – 8, and 12. These files can be opened with Wolfram Inc.'s free cdf player, see https://www.wolfram.com/cdf-player/.
[34] K. Binder and A. P. Young, *Spin Glasses: Experimental Facts, Theoretical Concepts and Open Questions*, Rev. Mod. Phys. **58**, 801 (1986).
[35] G. Korniss, M. A. Novotny, H. Guclu, Z. Toroczkai, and P. A. Rikvold, *Suppressing Roughness of Virtual Times in Parallel Discrete-Event Simulations*, Science **299**, 677 (2003).
[36] M. A. Novotny and G. Korniss, "*Fully scalable computer architecture*," US patent 6,996,504.
[37] Mississippi State University, patent pending.
[38] R. T. Scalettar, *Critical properties of an Ising model with dilute long range interactions*, Physica A **170**, 282 (1991).
[39] M. Gitterman, *Small-world phenomena in physics: the Ising model*, J. Phys. A: Math. Gen. **33**, 8373 (2000).
[40] A. Barrat and M. Weigt, *On the properties of small-world network models*, Eur. Phys. J. B **13**, 547 (2000).
[41] A. Pekalski, *Ising model on a small world network*, Phys. Rev. E **64**, 057104 (2001).
[42] H. Hong, B. J. Kim, and M. Y. Choi, *Comment on "Ising model on a small world network*, Phys. Rev. E **66**, 019101 (2002).
[43] C. P. Herrero, *Ising model in small world networks*, Phys. Rev. E **65**, 066110 (2002).
[44] X. Zhang, *Critical properties of small world Ising models*, Ph.D. thesis, Mississippi State University (2005).
[45] X. Zhang and M. A. Novotny, *Critical behavior of Ising models with random long-range (small world) interactions*, Braz. J. Phys. **36**, 664 (2006).
[46] D. J. Watts, *Small worlds: The dynamics of networks between order and randomness* (Princeton University Press, Princeton, N.J., 1999).
[47] R. Albert, H. Jeong, and A.-L. Barabási, *Internet: Diameter of the World-Wide Web*, Nature **401**, 130 (1999).
[48] R. Albert and A.-L. Barabási, *Statistical mechanics of complex networks*, Rev. Mod. Phys. **74**, 47 (2002).
[49] A. Barabási, *Network Science* (Cambridge University Press, Cambridge, U.K., 2016).
[50] M. Newman, *Networks* (Oxford University Press, Oxford, U.K., 2018).
[51] A. P. Young and H. G. Katzgraber, *Absence of an Almeida-Thouless line in Three-Dimensional Spin Glasses*, Phys. Rev. Lett. **93**, 207203 (2004).
[52] H. G. Katzgraber and A. P. Young, *Probing the Almeida-Thouless line away from the mean-field model*, Phys. Rev. B **72**, 184416 (2005).
[53] T. Jörg, H. G. Katzgraber, and F. Krzakala, *Behavior of Ising Spin Glasses in a Magnetic Field*, Phys. Rev. Lett. **100**, 197202 (2008).
[54] H. G. Katzgraber, H. Bombin, and M. A. Martin-Delgado, *Error Threshold for Color Codes and Random 3-Body Ising Models*, Phys. Rev. Lett. **103**, 090501 (2009).
[55] J. R. L. de Almeida and D. J. Thouless, *Stability of the Sherrington-Kirkpatrick solution of a spin glass model*, J.

Phys. A **11**, 983 (1978).
[56] G. Parisi, P. Ranieri, F. Ricci-Tersenghi, and J. J. Ruiz-Lorenzo, *Mean field dynamical exponents in finite-dimensional Ising spin glass*, J. Phys. A **30**, 7115 (1997).
[57] S. Boettcher, *Stiffness of the Edwards-Anderson Model in all Dimensions*, Phys. Rev. Lett. **95**, 197205 (2005).
[58] M. Demirtaş, A. Tuncer, and A. N. Berker, *Lower-critical spin-glass dimension from 23 sequenced hierarchical models*, Phys. Rev. E **92**, 022136 (2015).
[59] O. Melchert, *autoScale.py - A program for automatic finite-size scaling analyses: A user's guide*, Preprint: arXiv:0910.5403v1 (2009), the source-code of autoScale.py can be downloaded at http://arxiv.org/abs/0910.5403 by choosing the download-option `Other formats`.
[60] A. de Candia, A. Fierro, and A. Coniglio, *Scaling and universality in glass transition*, Nat. Sci. Rep. **6**, 26481 (2016).
[61] Bootstrap percolation studies the spread of 'infections' on graphs [66–68].
[62] K. Hukushima and K. Nemoto, *Exchange Monte Carlo method and application to spin glass simulations*, J. Phys. Soc. Jpn. **65**, 1604 (1996).
[63] H. G. Katzgraber, M. Palassini, and A. P. Young, *Monte Carlo simulations of spin glasses at low temperatures*, Phys. Rev. B **63**, 184422 (2001).
[64] *D-Wave Systems, Inc*, `https://www.dwavesys.com`.
[65] G. Barmpalias, N. Huang, A. Lewis-Pye, A. Li, X. Li, Y. Pan, and T. Roughgarden, *The idemetric property: when most distances are (almost) the same* (2018), (arXiv:cs/1804.11187).
[66] J. Adler, *Bootstrap percolation*, Physica A **171**, 453 (1991).
[67] S. Janson, T. Luczak, T. Turova, and T. Vallier, *Bootstrap percolation on the random graph $G_{n,p}$*, Ann. Appl. Prob. **22**, 1989 (2012).
[68] R. Morris, *Bootstrap percolation, and other automata*, Euro. J. Combinatorics **66**, 250 (2017).